Structural Analysis of MP3-Players

Fabio Bocchi & David B. Bogy

Computer Mechanics Laboratory
Department of Mechanical Engineering
University of California, Berkeley

September 13, 2012

Abstract

This project deals with numerical structural analysis of various mp3-devices. The continuing improvement of the size, performance and the manufacturing of such devices motivated our study. However, manufacturers are confronting a problem of keeping a necessary level of protection of their devices when they experience different types of mechanical loads and impacts. So we began a project to simulate the mechanical behavior of such devices, pointing out how the components inside, such as the battery or the printed circuit board (PCB), respond to different loadings.

First the static mechanical response of two such devices with different shell configurations was simulated using a real life loadings, such as someone, having a device in his back pocket, leaning against a handrail. This scenario is able to help us understand the way in which the components are deformed and which connections between components improve mechanical behavior.

Next, some drop test simulations were carried out. Indeed, impact of such devices after a fall is one of the most important causes of electronic equipment failure. So, we performed some drop test simulations such as bottom edge drop in order to determine which components are most sensitive to such loadings.

Since we simulated older, no longer manufactured devices, the main aim of this study is to generally show how numerical simulation can provide input into the design , development and manufacture of electronic devices.

Introduction

Nowadays, MP3-Players have become more and more compact, while increasing the performance of components such as battery life or processors power. This decrease of device size requires manufacturers to reduce the size of the components while keeping sufficient protection during extreme mechanical loading conditions. In this paper, we test the mechanical response of different components inside two different MP3-devices that have different casing configurations. One is a two-part body device with a stainless steel bottom and a polymer top. The other one is a unibody design made of aluminum.

In order to compare the mechanical behaviors of the two devices, we focused our study on two essential components : the battery and the circuit board. First, the static mechanical behavior of these two devices was accomplished with a real life loading. We simulated the case of a user, having a device in his back pocket, leaning against a handrail. We represent the handrail as a rigid fixed cylinder on which the device is in contact. The Figure 1 below shows this configuration.

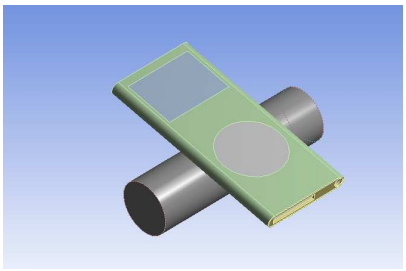

Figure 1: handrail configuration

Afterwards, some basic drop test simulations were achieved. Indeed, we simulated the real case of a fall i.e., a bottom edge drop on a rigid ground, as shown in Figure 2.

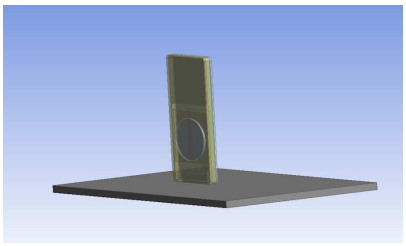

Figure 2: Bottom edge drop

The study was carried out using Ansys Workbench, a commercial finite element software. Ansys Mechanical was used for the static analysis and for the dynamic simulations, we used an explicit solver Ansys Autodyn.

Modeling

Two Finite Element (FE) models were built using Ansys DesignModeler, a CAD software included in Ansys Workbench. The components' sizes were measured using real MP3-devices, and we chose not to model such small parts and features as micro-processors bonded on the PCB, fillets, overhangs and holes . Indeed, our study is devoted to the structural analysis of MP3-players as a whole so we didn't focus on these components which may have a small effect on the results. Moreover, this approach can save computational time particularly for all the drop test simulations. In future work these could be taken into account to increase the accuracy.

Figure 3 shows the entire assembly (left) and components inside (right) of the two-part body device, and Figure 4 shows the same for the unibody device.

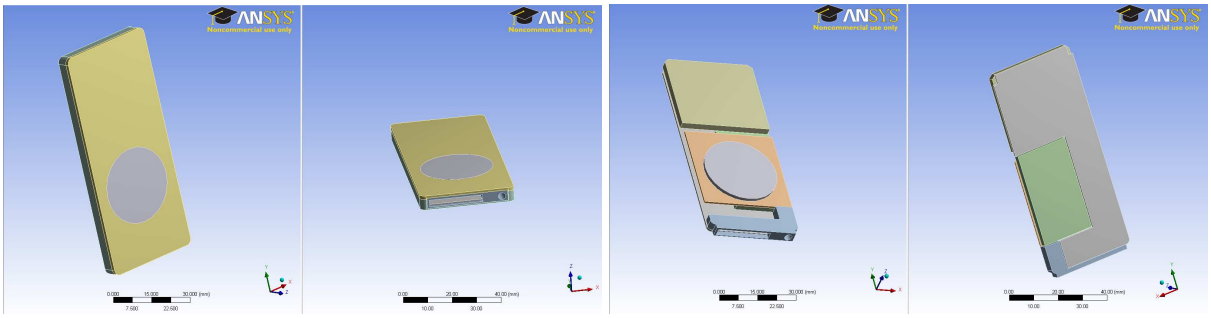

Figure 3: Two-Part Body Device Model

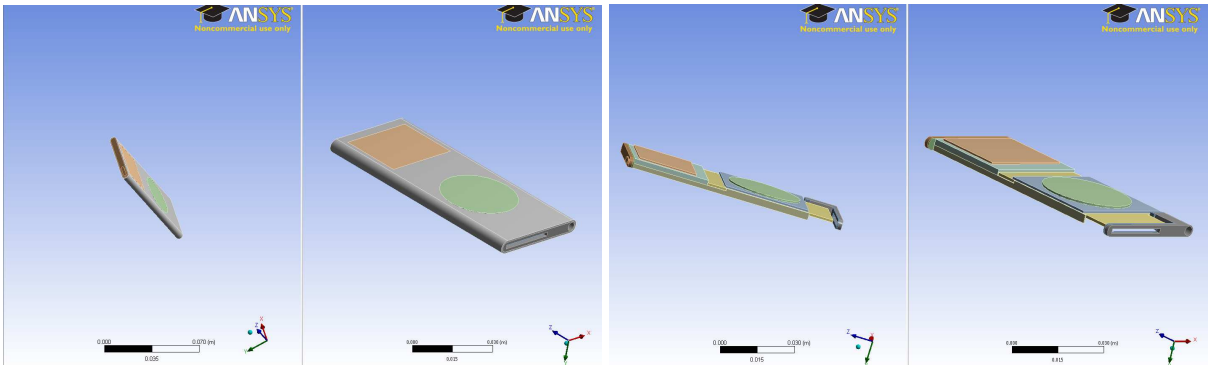

Figure 4: Unibody Device Model

Also, a more accurate model of the unibody device was made to carry out the drop test simulations on concrete. Indeed, some components such as the steel part around the PCB and the battery bonded on the top of the case were built more accurately (Fig. 5).

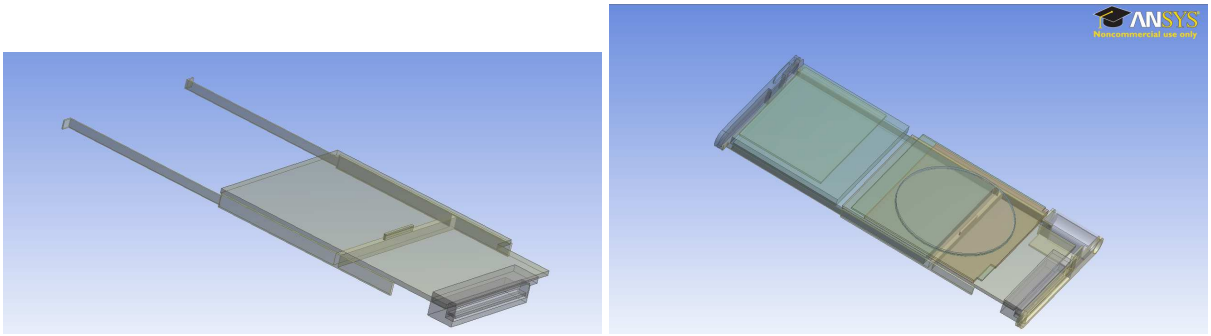

Figure 5: (a) PCB, Metal & Charger Part (b) Assembly

Next the materials composing each component of the modeled devices are defined. Due to IT concerns, data as to their material composition is very limited. Because of this, some hypotheses were made on materials used for our Finite Element Analysis (FEA). Table 1 below shows all the material properties (cf [7]) :

Material	Density (kg m^{-3})	Young's Modulus (GPa)	Poisson ratio	Tensile Yield Strength (MPa)	Compressive Yield Strength (MPa)	Tensile Ultimate Strength (MPa)	Compessive Ultimate Strength (MPa)
Aluminium Alloy	2770	71	0.33	280	280	310	/
Stainless Steel	7750	193	0.31	207	207	586	/
ABS	1050	2.34	0.27	435	/	318	/
PMMA	1180	3.3	0.37	/	/	80	/
Polycarbonate	1200	2.22	0.37	65	85	80	100
Polyethylene	950	1.1	0.42	25	/	33	/
FR-4	1850	18	0.118	280	390	320	420
Concrete	2300	30	0.18	0	0	5	41

Table 1: Material Properties

One of our aims is to compare the effectiveness of the case designs in protecting the internal components. Most of the internal components are similar between the two devices, so as long as the materials are consistent between the two devices, the relative effectiveness of one case to the other should be preserved. For instance the Battery, PCB and Screen are similar in the two devices. Polyethylene was used in the battery in both devices. Whereas, the PCB and Screen are made of FR-4 and Polycarbonate respectively.

Finite Element Method & Computational Contact Mechanics

The classical linear system in the finite element method that must be solved can be written as :

$$[K]\{u\} = \{F_a\} \tag{1}$$

where : $[K]$ is the Stiffness Matrix, $\{u\}$ is the Vector of unknown DOF, $\{F_a\}$ is the Vector of applied loads

This kind of linear systems is solved using a sparse direct solver based on the LU decomposition implemented in the finite element commercial software ANSYS. But one of the biggest issues is the computational contacts which makes the $[K]$ Matrix depend on $\{u\}$. So, in this case, one must solve a nonlinear system. The Newton-Raphson (NR) Method is used to accomplish this job. The nonlinear equation is written as :

$$[K]_i\{\Delta u_i\} = \{F_a\} - \{F_i^{nr}\} \tag{2}$$

where : $[K]_i$ is the Jacobian Matrix, $\{\Delta u_i\}$ is the vector of incremental DOF, $\{F_a\}$ is the vector of applied loads, and $\{F_i^{nr}\} = [K]_{u_i}\{u_i\}$ is the vector of restoring loads

At the end of each iteration, the vector of DOF is updated as :

$$\{u_{i+1}\} = \{u_i\} + \{\Delta u_i\} \tag{3}$$

and the residual load is computed from :

$$\{R\} = \{F_a\} - \{F_i^{nr}\} \tag{4}$$

The latter equation was used for the convergence criteria. The NR loop stops when the residual is much less than 0.1% of the applied loads ($||R||_{L^2} < 0.001||F_a||_{L2}$). Then, a similar criteria was applied for displacement convergence.

Furthermore, sometimes using the whole vector of incremental DOF causes some instabilities. So, a line search parameter algorithm was used to avoid this problem. The previous updated vector of DOF is modified as :

$$\{u_{i+1}\} = \{u_i\} + s\{\Delta u_i\} \tag{5}$$

where s is a scalar value found by minimizing the energy potential of the system which is reduced to find the zero of the function below :

$$gs = \{\Delta u_i\}^T(\{F_a\} - \{F_i^{nr}(s\{\Delta u_i\})\}) \tag{6}$$

Given that this is a 1D function, the Regula-Falsi method was efficient and chosen in ANSYS. Moreover, convergence difficulty due to an unstable problem is usually the result of a large displacement for smaller load increments. Nonlinear stabilization in ANSYS can be understood as adding an artificial damper element at each node of an element. ANSYS calculates the damping force such that it is proportional to a relative pseudo velocity which is calculated as the displacement increment divided by the time increment of the substep. Therefore for any DOF that tends to be unstable because of a large displacement increment

causing a large damping (stabilization) force; this force, in turn, reduces the displacements at the DOF so that stabilization is achieved.

$$\{F\} = -C\{V\} \tag{7}$$

where : $\{V\}$: pseudo velocity, C : virtual damping coefficient

For the stable DOFs, this method has a little effect on the results because the stabilization forces are much smaller than the real forces. Nevertheless, one must be careful about the value of the virtual forces. Indeed, if these are not much less than the physical forces, the results could be inconsistent. That's why, at the end of each sub step the values are checked and compared. If the virtual force values are more than 10% of the real ones, then the simulation stops.

An important issue in the analysis of a multi-body system such as an electronic device is the method for computing contacts that are often nonlinear. First, one has to choose a formulation and a detection method to solve these problems. We chose the augmented Lagrange method based on both the Pure Penalty method and the Pure Lagrange method. That means both a penalty coefficient and a Lagrange multiplier are used. The advantage of this method is that it enables a reduction in penetration compared to the pure penalty method, and it provides faster convergence than the pure Lagrange method. For more details, the reader can refer to [3] & [5]. The Detection method allows us to choose the location of contact detection used in the analysis in order to get a good convergence. Usually when the formulation is set to Augmented Lagrange or Penalty, the detection based on Gauss integration points is the more accurate.

Moreover, because of the way of modeling the component parts in CAD softwares, some small penetrations or gaps between two different parts can sometimes occur when it's not expected. To deal with this, a method called "adjust in touch" in ANSYS was used. One can understand this method as one in which any initial gap or penetration is ignored by the solver so that the results can be more consistent and closer to the boundary conditions used. For more information about the contact result tracker during a simulation see [2]. An example of the Newton-Raphson force convergence evolution during a simulation is shown in Figure 6.

Finally, our drop test simulations were carried out by using an explicit solver. To monitor the consistency of the results during the simulation, we followed the energy conservation graph. If an error of more than 10 % in the energy conservation occurs, the simulation stops (the first energy value was taken as the reference energy). An example of this is shown in Figure 7. Here, the energy error is less than 6% of the reference energy. Furthermore, The properties for contact interaction for this explicit solver are quite different compared to the mechanical APDL solver used in the static analysis. First, the detection method used in this case is called "trajectory". The trajectory of nodes and faces are reviewed during the computation. If the trajectory of a node and a face intersects during the simulation a contact event is detected. This method is chosen for its accuracy and efficiency. Nevertheless, any nodes which penetrate into any other elements at the beginning of the simulations will be ignored for contact problems. To avoid this issue refer to Shared Topology in [3]. In case a contact is detected, a penalty force is computed to hold off the node in contact with the face.The purpose of this force is to push the node back in order to put it towards the true contact position, but this is not completely reliable so one must check the penetrations between different parts during the simulation to make sure that the results are reliable. ANSYS computes

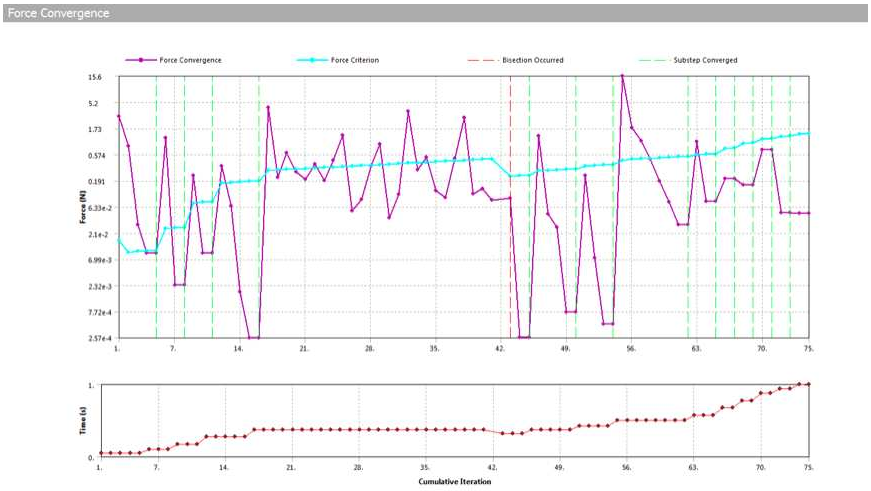

Figure 6: NR Force Convergence

this force as :

$$F = 0.1 \frac{M_N M_F}{M_N + M_F} \frac{D}{\Delta t^2} \tag{8}$$

Where D is the penetration depth, M_N is the mass associated to the node in contact, M_F is the mass associated to the face in contact and Δt is the time step.

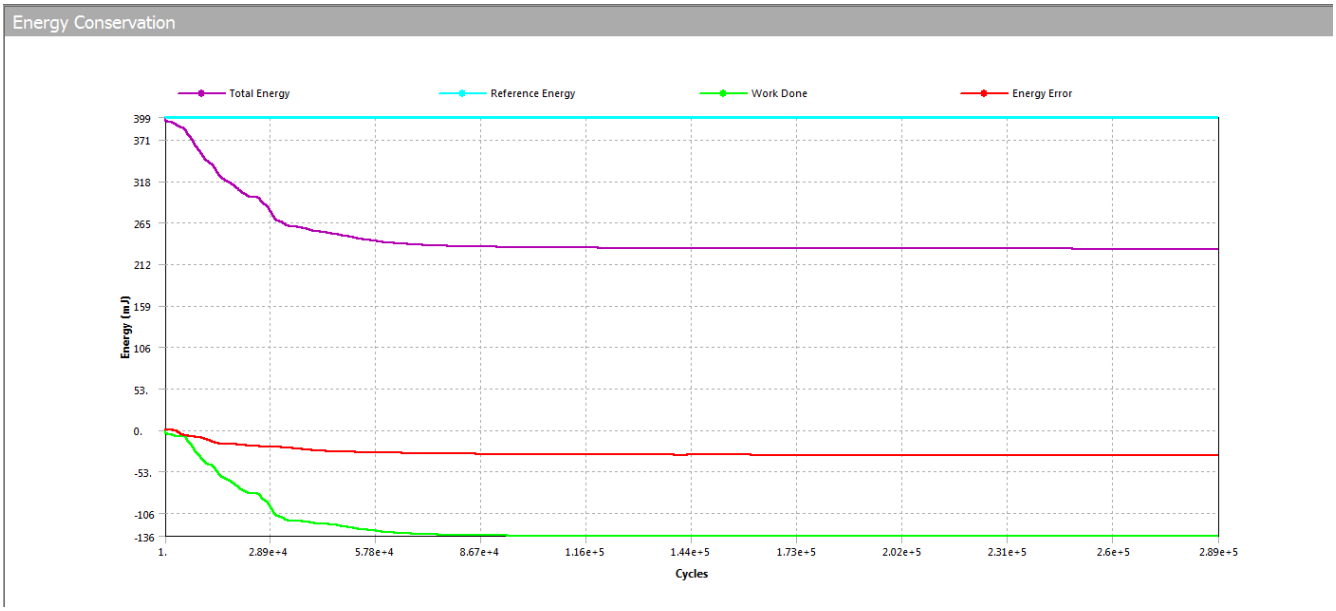

Figure 7: Energy Conservation

Simulations Results

Static Analysis

The case of someone having a device in his back pocket, leaning against a handrail was modeled. The handrail was modeled as a rigid cylinder fixed on its extremities. To represent a real life loading, a uniform pressure of 0.3 MPa is applied on the entire front surface (a loading equivalent to a person weighing 80 kg). To get convergence, one must apply this load as ramped up in time. Indeed, if one were to apply a constant 0.3 MPa pressure on the whole front surface, changes in contact status would be too large. The NR loop could be infinite, and divergence could then occur.

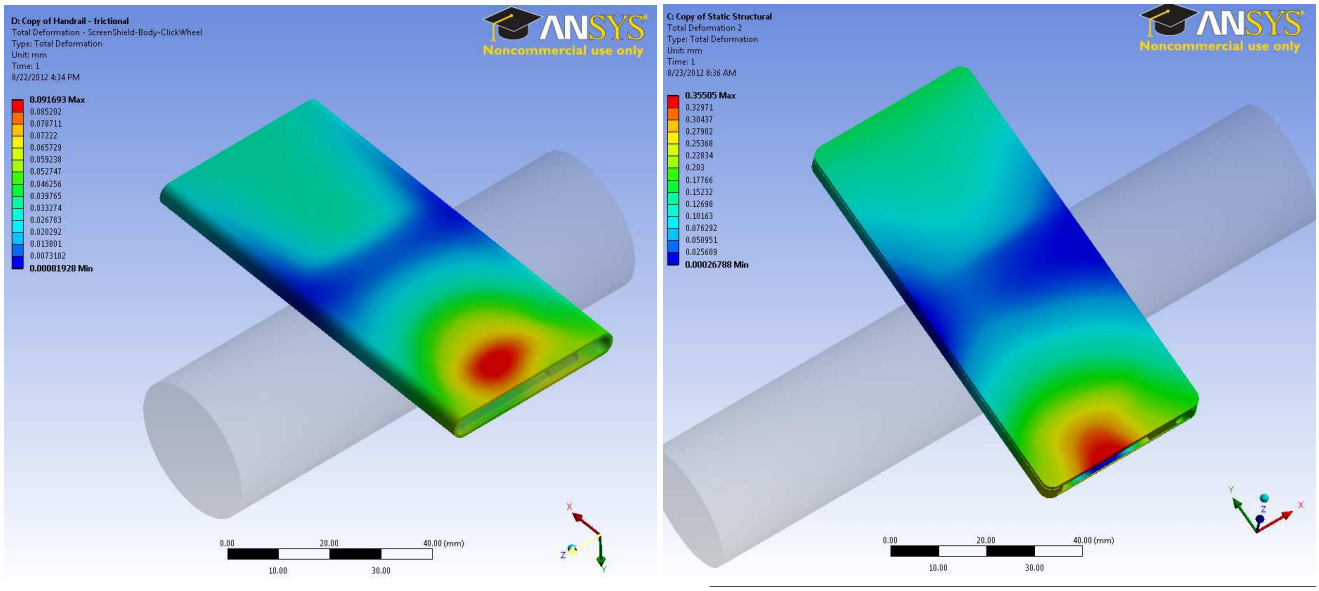

Figure 8: (a) Displacement unibody (b) Displacement two-part body

Figure 8 shows the displacements of the both devices. One can see that the profiles look similar in the two devices. However, the scale-value is quite different between same. In fact, in the same areas, the displacement over the two-part device is almost 4 times larger than over the unibody. Actually, looking at the displacement is not very useful, but it allows one to have idea of the results consistency. Indeed, it's easier to have physical intuition about displacement than about strains or stresses. First, the differences between the values in the two devices can be explained by the differences in the materials used. Recall that the unibody is made of Aluminium where as the front of the other one is ABS (a kind of plastic). Furthermore, the maximum values are located at the regions provided intuitively. The bottom of each devices is less rigid, because of the clearance between the components inside (one can refer to the picture in the modeling section). Having checked the results consistency, we are able to focus on the strains and stresses which are expected to be larger in the contact region between the device and the handrail. Figure 9 shows the equivalent stress on the back face of each device. As we can see, the Von-Mises stress is relatively large in this area. Nevertheless, the average element size in this contact region is about 0.8 mm which is probably a little too large to get the real contact area that would be smaller than the one obtained. Nevertheless, the results are close enough to the expected ones since the impact of this error

on the internal components is low. Here also, one observes that equivalent stress is also larger on the two-part body device.

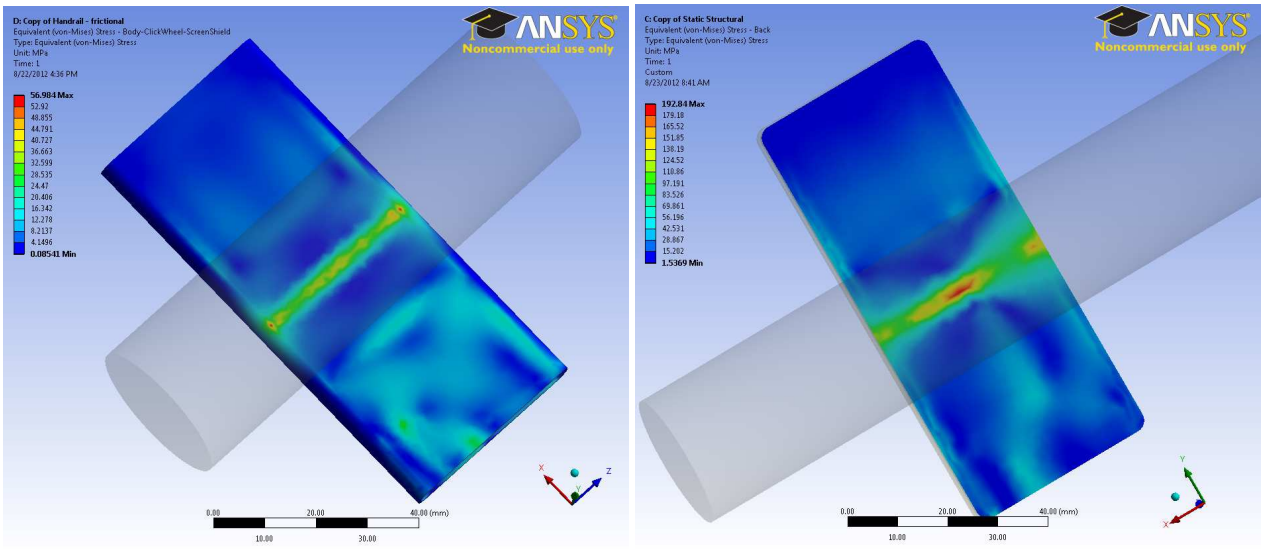

Figure 9: Stress over back face - (a) unibody (b) two-part body

Before showing the results on the inside components, one interesting thing to emphasize is the Von-Mises stress profile in the contact region between the front and the back of the two-piece device. In fact, as shown in Figure 10, large stresses occur in this region and the two parts tend to be separated and the contact broken. The stress profile along the path peaks at the cylinder contact region with a maximum value around 392 MPa. Overall, the two-part device experiences much larger stresses than the unibody device in this loading example.

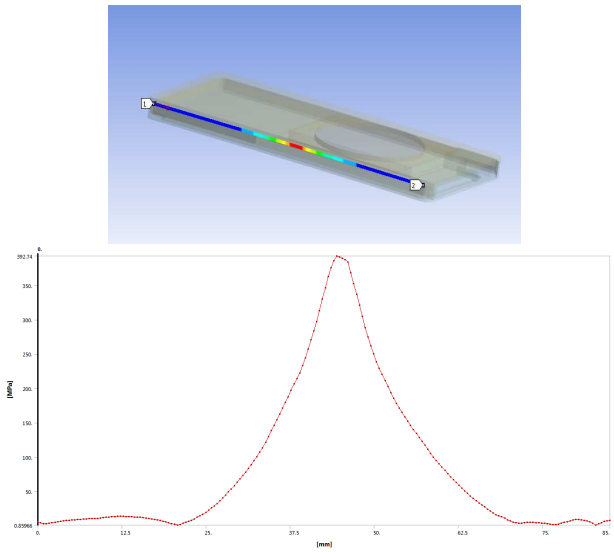

Figure 10: (a) Von-Mises Stress (b) Path (c) Von-Mises Stress along the path

The contact between the front and back is modeled as a frictional contact with a 0.7 coefficient. In reality, the two parts are not only held together using a friction coefficient, but also by fasteners forced into a locked position. But modeling a contact like that requires use of a much finer mesh which increases the computational time. We modeled it as a frictional contact with a coefficient that represents to some extent the rigid link between these two different parts. One must be aware that the obtained values for displacements and stresses are probably not exactly the same as they would be in real conditions. But even if the values should be somewhat different, the mechanical behavior will not be much affected by this simplified approach so the stress profile is expected to be similar and values in this region of contact would remain still larger than the stress on the other areas of the device.

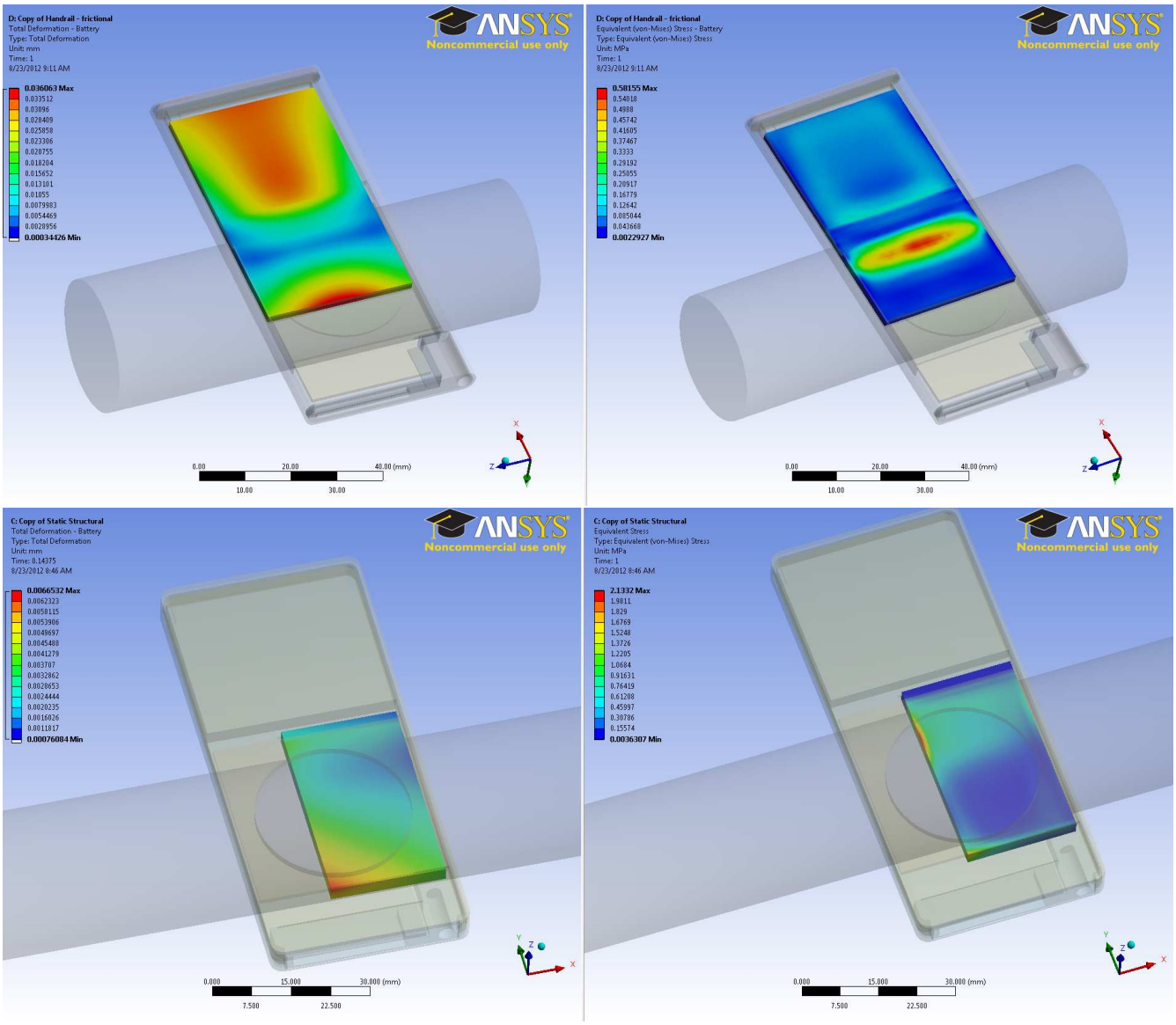

Figure 11: (a) Displacement (b) Equivalent Stress (c) Displacement (d) Equivalent Stress

Next we focus our attention on the Battery. First, on the left side of Figure 11 the battery displacements on both devices are shown to check the consistency of the results. There is no displacement in the contact

region between the device and the handrail. Moreover, closer to the bottom or top, stresses are more important. That is expected because with such loading a flexure type loading occurs in the region of the contact with a kind of fixed boundary condition where the contact occurs. In terms of Equivalent Stresses (on the right of Figure 10), in each device large stresses occur in the contact area where the device is in contact with the handrail. But the values are still quite different between the two device. Indeed, the stress over the battery inside the two-piece device is around 4 times greater than inside the unibody one. Nevertheless, as shown in Figure 12, the maximum value is less than 0.6 MPa and compared to Yield Strength and Ultimate Strength of the polyethylene (Table 1 Section Modeling) used for the battery, the maximum value is enough below those two values to conclude that the battery is resistant enough to such loading in both cases.

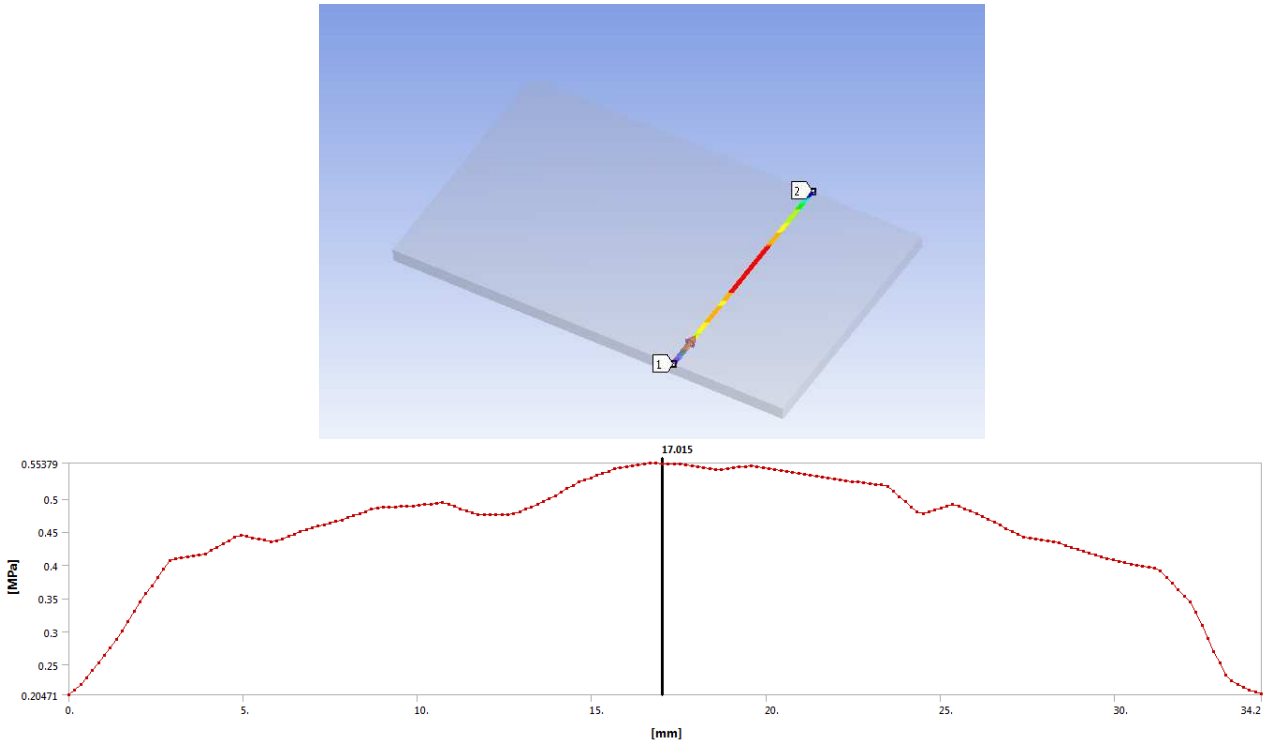

Figure 12: (a) Path on battery (b) Equivalent Stress along the path

Finally, the biggest differences between the two devices, except the case, in terms of components, is the steel part around the PCB, the Battery and the Screen inside the unibody device. Figure 13 shows the equivalent stress on this part. Large stresses occur (maximum around 62 MPa) which are much greater than the stresses on the other components inside. Presumably this component is included and designed to decrease stresses on other parts inside the device. Indeed, this part stores relative large stresses which are not reflected on useful components such as the Battery or PCB so that the components inside this device are less sensitive to such loadings.

According to these results, It can be concluded that the unibody device is much more rigid than a two-piece device. First, the shell of a unibody is more resistant. Furthermore, some improvements inside the

device were included (such as the Steel Part) between the first generation (two-part piece) and the second generation (unibody) in order to improve the mechanical response of the components inside.

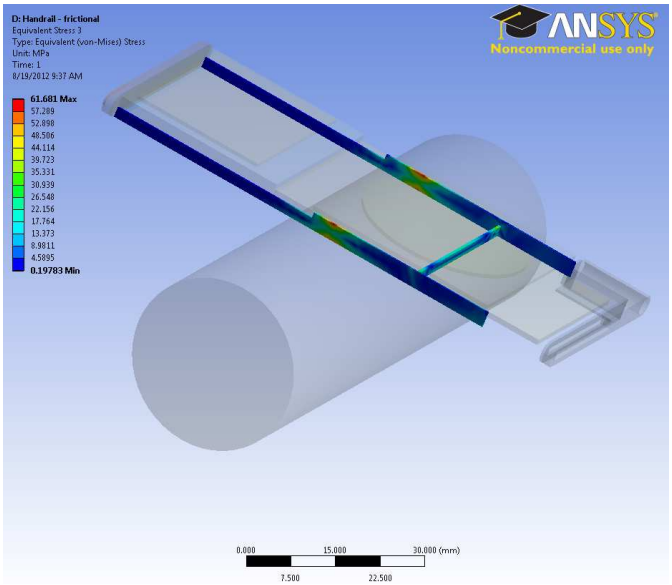

Figure 13: Unibody Steel Part

Dynamic Analysis

With the continual increase of electronic devices in our daily lives such as the cell-phone, tablet, mp3-players, etc., drop tests have become more and more useful in the manufacturing process. Here we simulated some drop tests of the two mp3 players on concrete. Since an explicit solver was used, one must pay attention to the time step to get convergence, and also to get consistent results with real mechanical phenomena. First, we can expect to see a propagating wave of stress or strain after the shock or impact between the device and the ground. For instance, waves propagate in metals at around 5000 $m.s^{-1}$ equivalent to 5 $mm.\mu s^{-1}$, and since the devices are around 95 mm high, using a time step of 1 μs should be small enough so that this phenomenon can be seen. Moreover, the explicit solution is only stable if the time step size is smaller than the critical time step size based on Courant-Friedrichs-Levy (CFL) criterion:

$$\Delta t \leq \Delta t_{crit} = \frac{2}{\omega_{max}} \tag{9}$$

where ω_{max} is the largest natural circular frequency.

Here, ω_{max} is taken to be :

$$\omega_{max} = 2\frac{c}{I} \tag{10}$$

where I is a characteristic length and c is the wave velocity.

To get an idea of the magnitude of Δt_{crit}, one can choose the parameter I as the minimum edge length and choose the material which has the maximum velocity. In our case, I=0.250 mm and c=6400 $m.s^{-1}$ (Aluminium) so $\Delta t_{crit} = 3.9e^{-8}$ s. In order to be sure that the CFL condition is fulfilled, we have chosen

a time step of $1.0e^{-8}$ s. This is also small enough to satisfy the propagating waves condition mentioned above. Using an explicit solver such as Ansys Autodyn or LS-Dyna requires large computational time because such small time-step is needed, so we limited ourselves to short transient simulations (< 10 ms). Since the impact duration in a drop test is usually in the range of 0 to 5 ms, depending on the ground property, we chose a simulation duration of 3 ms, representing impact on concrete. Moreover, the simulations are performed in such a manner that a drop test of around 1.6 m high is carried out. So the initial impact velocity can be compute as :

$$v = \sqrt{2gh} \tag{11}$$

Finally, frictionless and frictional Body Interaction are used in addition to the contacts defined and already analyzed in the previous section. This interaction type applied to all bodies activates frictionless contact between any external node and face that may come into contact in the model during the analysis. But in order to improve the efficiency, it is advised to remove the default frictionless interaction that is applied to all bodies, and instead add Body Interaction objects which limit interaction(s) to specific bodies. Moreover, if the bonded contact between two faces or bodies breaks during the simulation, we want frictional or frictionless contact to take place between these two faces or bodies. For instance one can imagine that during the drop test the bonded contact between the headphone jack part and the bottom of the front of the two-piece body device could be broken, and so we want a different type of contact to take place. A frictional or frictionless body interaction type applied between these two faces will achieve this.

When looking at the Von-Mises stress distribution or the displacements during the drop test, animation is by far the best way to display the results. Here, the Equivalent stress distribution may be viewed at impact to compare the reaction of these two devices in terms of mechanical response. This is shown in Figure 14. The stresses are concentrated on the bottom of each device after the impact. However, the profile and the values are quite different in each of them. As it was for the static analysis the two-piece device is more sensitive to such loading. Moreover, it is interesting to look at the graphs below the picture. These two graphs represent the maximum values of the equivalent stress with respect to time. We can see that on both devices large stresses occur at the impact and decline quickly afterwards. We can also mention that the maximum equivalent stress occurs earlier on the unibody device (at $2.0e^{-5}$ s) than on the two-part device (at $5.0e^{-5}$ s). Also, as mentioned above the short duration of the impact is confirmed by these two graphs, and the rapid increase of the equivalent stress in a short time causes the failure of contacts between the front and the back of the two-piece device and between the head phone jack part and the front. This contact failure is shown in Figure 15 for both simulation and experiment. The numerical results appears to be close to the reality. However, our project is limited to numerical analysis, this photo is presented to show the consistency of our results with experiments if one wants to compare in details of the simulation results with the experimental results.

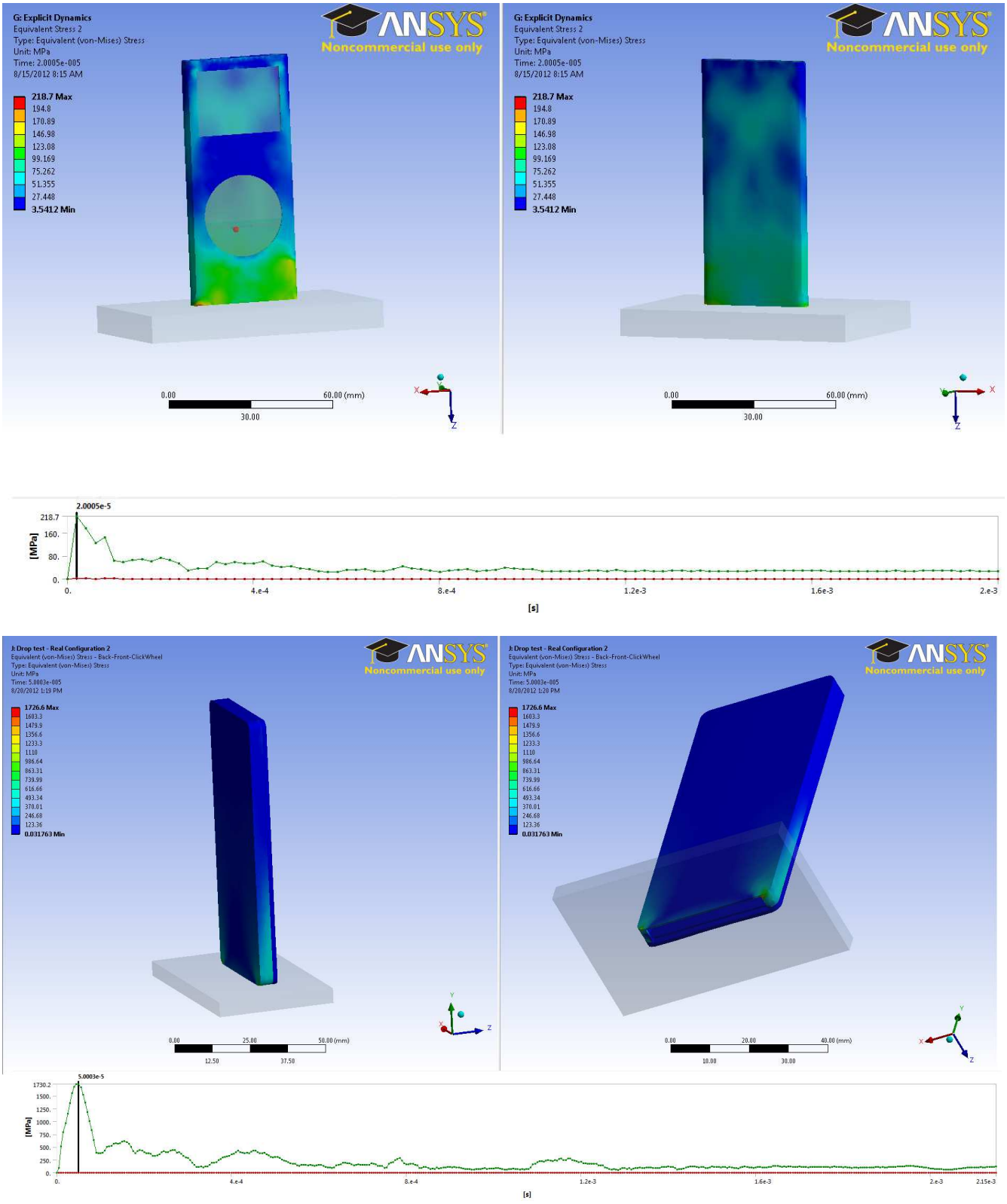

Figure 14: Equivalent Stress distribution at impact (a) Unibody (b) Two-piece device

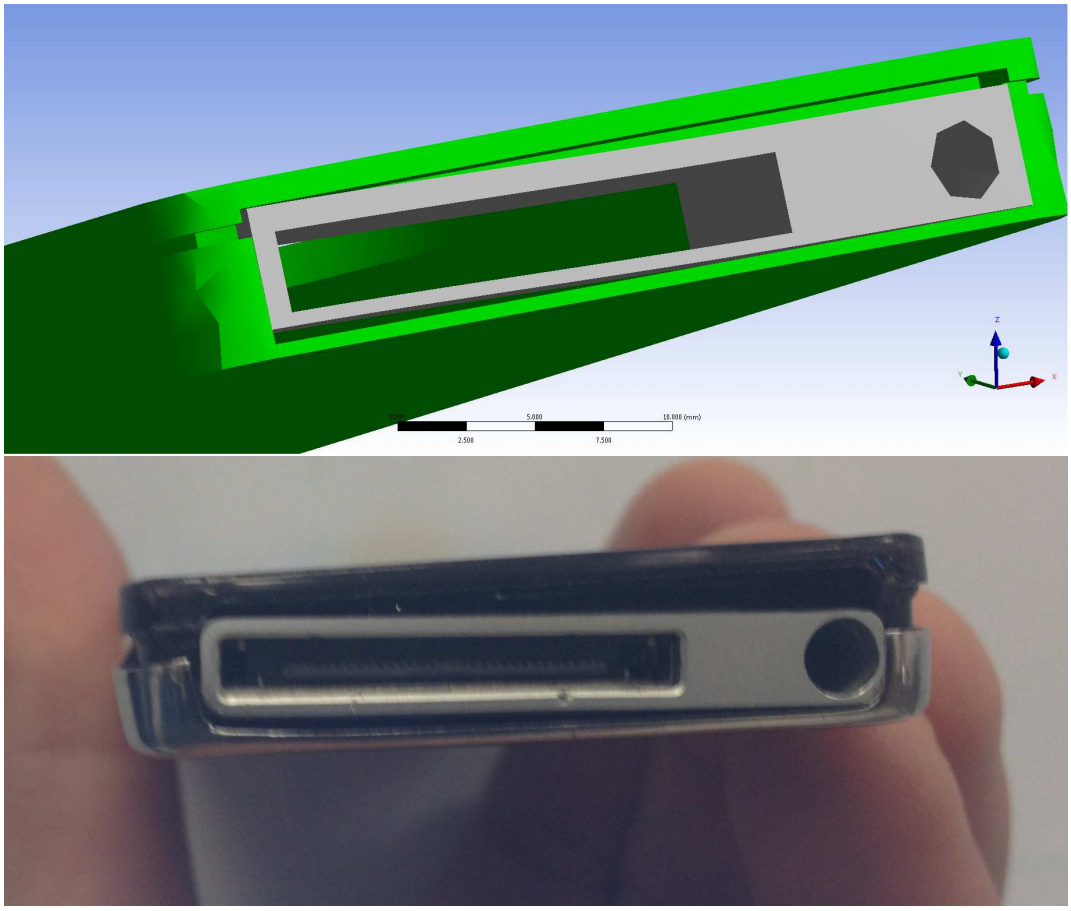

Figure 15: Contact failure

The next step is to emphasize the way in which the inside components are deformed during the drop test. Figure 16 shows the equivalent stress on the PCB (on the left) and the Battery (on the right) on each device. According to the stress values, the PCB is highly stressed in both cases. The distribution is homogenous and in view of the results, plasticity can occur on this part after the drop impact. Moreover, because of the boundary condition between the PCB and the charger part in the two-piece device larger stresses occur on the PCB inside this device. Indeed, the charger part comes into contact with the ground at impact, the stresses propagate quickly over the PCB and lead to significant deformations. Moreover, the results on the battery are quite different in the two devices. This is explained by the different boundary conditions acting in both cases. The stresses on the battery inside the unibody device are only concentrated in the area where it is bonded with the PCB, whereas in the other device, the Von-Mises stress is almost homogenous.

In order to show the propagating waves on the shell after the impact the equivalent stress is displayed at different times in Figure 17. As we can see on these pictures the time it takes the waves to reach the top of the device is about 16 μs. In theory, the velocity of longitudinal waves for an isotropic material is calculated as :

$$c_l = \sqrt{\frac{E(1-\nu)}{\rho(1+\nu)(1-2\nu)}} \tag{12}$$

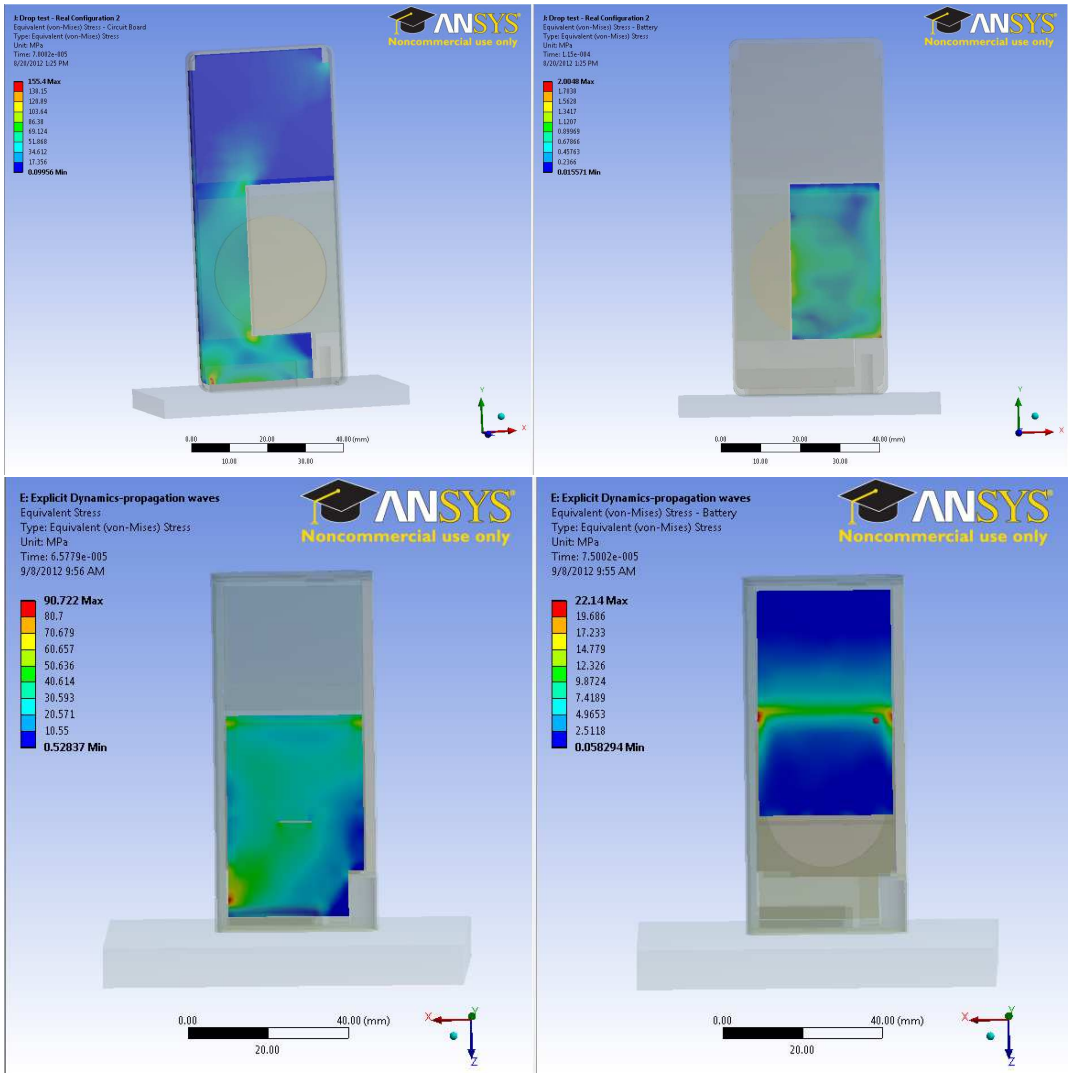

Figure 16: Equivalent stress on inside components

where E is the Young's modulus, ρ is the density and ν is the poisson ratio.

Taking into account the values given in Table 1, $c_l = 6163\ m.s^{-1}$ i.e $c_l = 6.163\ mm.\mu s^{-1}$ for the aluminum. Given that the unibody device is 95 mm high we can expect that the waves take 15.4 μs to reach the top. Comparing this to the simulation value we can see that it gives a relative error of about 3.8%. One can consider that this is not so far from the expected result. However, although this error is small, it should be even lower to be considered as satisfactory in a development process. Nevertheless, our dynamic study gives insight into all the mechanical phenomena that could be present in such loading, and it gives a good insight into the mechanical response of the components.

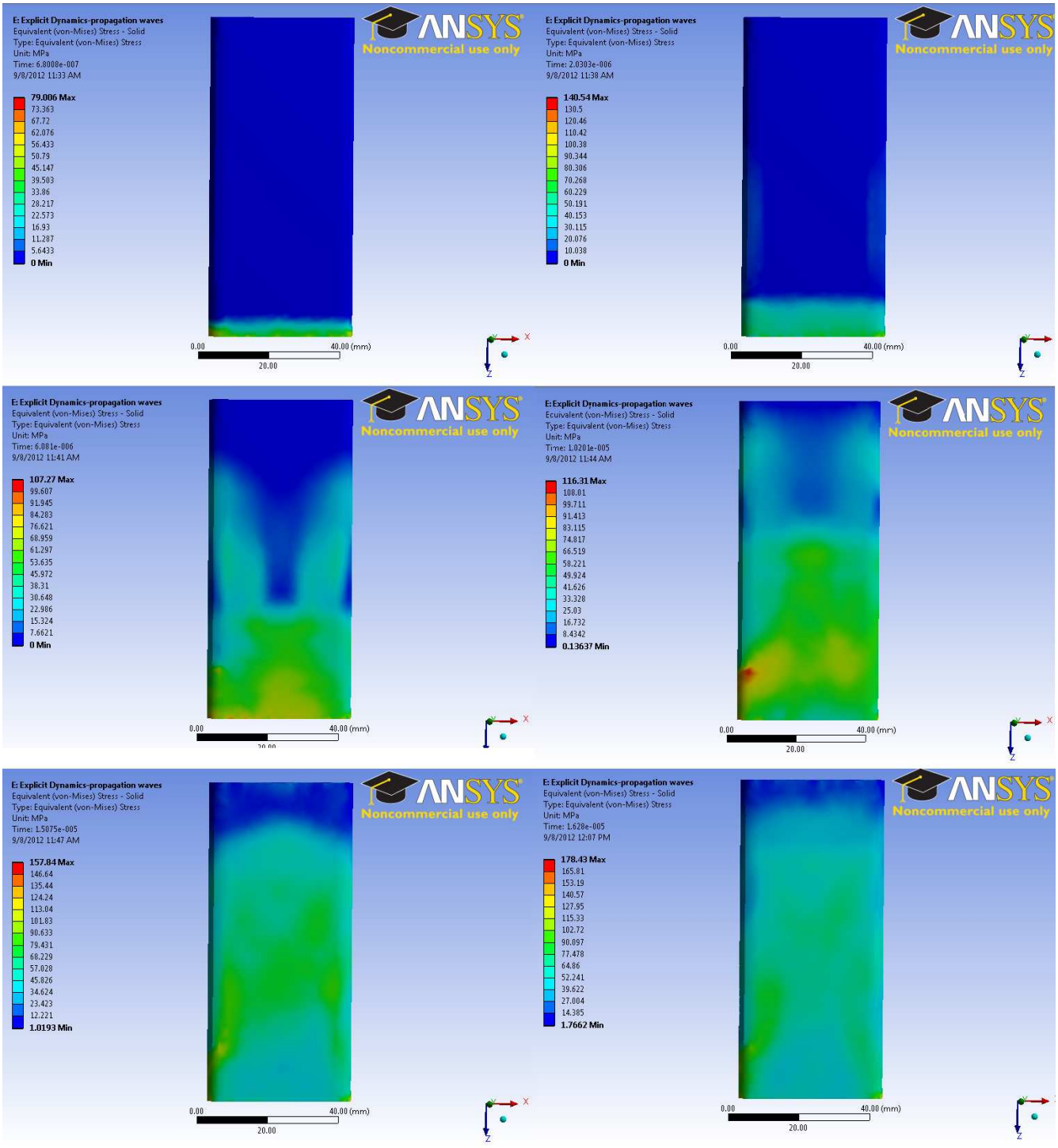

Figure 17: Equivalent stress back unibody (a) 0.6 μs (b) 2 μs (c) 6 μs (d) 10 μs (e) 15 μs (f) 16 μs

Conclusion

The main purpose of this study, which was to simulate the mechanical response of two different MP3-players and to compare the efficiency of two different shell configurations was achieved. However, some improvements can be made. First, in order to more accurately represent the real case, a more accurate model could be built taking into account the small components such as the overhangs, the holes and the resistors attached to the PCB. This will result in having to drastically reduce the size of the elements of the mesh and thus increase the computation time. Then, a parallel solver should be used and the use of the GPU would be a plus. But, some of the numerical methods used in this study are not available using GPU so modifications must be done. Moreover, it would be interesting in carry out some simulations after changing the configuration of the components inside the devices in order to know which could be the more robust in terms of mechanical response. Furthermore, with the aim of checking the consistency of the results it would be interesting to perform real experiments as well as simulations with another solver such as LS-Dyna or Abaqus.

Acknowledgments

This work was supported by the Computer Mechanics Laboratory in Mechanical Engineering Department at UC Berkeley. Financial support for the author Fabio Bocchi's study in University of California, Berkeley was provided in part by ENSEIRB-MATMECA.

References

[1] Anders Harryson. Drop Test Simulation of Cellular Phone. PhD thesis, Lund University, Sweden, 2003.

[2] Ansys Inc. Analyzing nonlinear contact. Ansys Advantage, 2009.

[3] Ansys Inc. Mechanical Application User's Guide. Ansys Inc, 2012.

[4] Cécile Lacroix. Modelisation of screen rupture during a mobile phone free fall. In 6^{th} European LS-DYNA User's Conference.

[5] T.A Laursen. Computational Contact and Impact Mechanics, Fundamentals of Modeling Interfacial Phenomena in Nonlinear Finite Element Analysis. Springer, 2002.

[6] Wei Liu & Hongyi Li. Impact analysis of cellular phone. In 4^{th}*ANSA*&μETA International Conference, 2010.

[7] Werner Martienssen & Hans Warlimont. Condensed Matter and Materials Data. Springer, 2005.